Analytical Biochemistry 654 (2022) 114777

Contents lists available at ScienceDirect

Analytical Biochemistry

journal homepage: www.elsevier.com/locate/yabio

Development of quantum dot-phthalocyanine integrated G-quadruplex /double-stranded DNA biosensor

Ayşe Topcu [a], Esra Bağda [a,*], Tülay Oymak [a], Mahmut Durmuş [b]

[a] Department of Basic Pharmaceutical Sciences, Analytical Chemistry Division, Faculty of Pharmacy, Sivas Cumhuriyet University, 58140, Sivas, Turkey
[b] Gebze Technical University, Department of Chemistry, Gebze, 41400, Kocaeli, Turkey

ARTICLE INFO

Keywords:
G-quadruplex
Quantum dot
Phthalocyanine
Biosensor

ABSTRACT

In the present study, the phthalocyanine (**Pc**) integrated mercaptopropionic acid capped quantum dot (**mpa@QD**) biosensor has been developed for the quantitative determination of G-quadruplex and double-stranded DNA. The working principle of the developed biosensor platform is based on the quenching of the emission signal of the **mpa@QD** in the presence of **Pc** (closed position) and the recovery of the fluorescence signal in the presence of DNA (open position). The parameters affecting biosensor performance, such as **Pc** type and concentration, were optimized. Since the developed biosensor aimed to determine G-quadruplex and double-stranded DNA in biological samples, the effect of common ions (such as Na^{+}, Mg^{2+}) and serum albumin found in many biological matrices on the biosensor performance were examined. The effect of common ions on biosensor signal was negligible, except Zn^{2+}. The analytical properties of the biosensor, such as linear range, calibration sensitivity, relative standard deviation %, the limit of detection, and quantification, were determined. The limit of detection and quantification values were found 0.055 μM and 0.18 μM for **AS1411**, 0.061 μM and 0.20 μM for **Tel21**, 0.038 μM and 0.13 μM for **Tel45** and 0.091 μM and 0.30 μM for **ctDNA**. Several different synthetic samples were prepared. The spiked synthetic samples such as mammalian cell medium were used to evaluate the analytical performance of **Pc-mpa@QD**. All synthetic samples were prepared with polyethylene glycol, which resembles biological samples' crowded environment.

1. Introduction

Quantum dots are often called fluorescent semiconductor nanocrystals consisting of groups II-VI, III – V, or IV metals in the periodic table. These attractive nanocrystals smaller than 10 nm in size were first discovered in a glass matrix by Alexey Ekimov in 1981. Louis Brus synthesized the first colloidal semiconductor nanocrystal solution four years later. QDs have unique structural, electrochemical, and photochemical properties [1]. These zero-size nanomaterials can be easily functionalized through surface modifications [2]. They are conjugated via a bridge or directly electrostatically and covalently. QDs can be dispersible in water by coating with functionalized silica, phospholipid micelles, and binders, such as mercaptoacetic acid, dihydrolipoic acid, or amphiphilic polymers [3,4]. Quantum dots provide several advantages over conventional fluorescent organic dyes in terms of narrow emission spectra, high fluorescence intensity, high quantum efficiency, adjustable excitation spectra, and photo-stability. These unique materials are used in fluorescence probing, imaging, and sensing applications with their size-dependent strong photoluminescence in different areas, such as the production of light-emitting diodes and solar cells [5–9].

QDs are considered promising fluorescent probes for a wide variety of analytes. Adegoke and Nyokong investigated many different QDs decorated with a variety of molecules for the determination of inorganic and organic biologically important analytes such as mercury [10], floride [11], and cysteamine and t-butylhydroperoxide, GSH, $HClO_4$ and ·OH radical [12]; bromide [13], peroxynitrite [14], H_2O_2 [15], superoxide anion [16] and hydroxyl radical [17]. The biomedical imaging applications of quantum dots are also widely employed [18]. QD-based probes were used for the first time in 1998 for *in vitro* biological imaging. Wu et al. have been developed QDs linked to immunoglobulin G (IgG) and streptavidin to label the breast cancer marker Her2 on the surface of fixed and live cancer cells, to stain actin and microtubule fibers in the cytoplasm, and to detect nuclear antigens inside the nucleus [19]. QD-based fluorescent probes are also gaining importance for monitoring the interactions of various cellular proteins. Jaiswal et al. have been developed specific protein tagging approaches based on QD to label

* Corresponding author.
E-mail address: esraer@cumhuriyet.edu.tr (E. Bağda).

https://doi.org/10.1016/j.ab.2022.114777
Received 21 March 2022; Received in revised form 31 May 2022; Accepted 8 June 2022
Available online 21 June 2022

living cells [20]. Gao et al. reported the multifunctional nanoparticle probes based on semiconductor quantum dots (QDs) for cancer targeting and imaging inzliving animals [21]. Zhao et al. have been developed reversible fluorescence "turn-off-on" sensor based on quantum dots (QDs) for the investigation of the interactions between TMPyP and different DNAs (double-stranded DNA, single-stranded G-quadruplex, and various types of G-quadruplexes) in Na^+ or K^+-containing buffer for the determination of the interactions of anticancer drugs [22].

Guanine-rich DNA sequences can form non-canonical structures known as G-quadruplexes. G-quadruplex-forming guanine-rich DNA sequences are found in the genome's important parts, such as at the ends of the telomeres, ribosomal DNA, and oncogene promoters [23]. These structures *in vivo* conditions have been discovered, and their quantitative determination in various biological environments has gained importance to determine their roles in metabolism. The discovery of unique secondary DNA structures and speculation about their potential functions in the living organism has brought attention to recognizing the specific DNA structure [24].

Quantum dots can significantly improve the analytical performance of biosensors, such as detection limit, sensitivity, and selectivity. In the present study, a **Pc-mpa@QD** biosensor was developed. Pc compounds were used due to their planar structure and high ability to establish strong π–π stacking interactions with G-quadruplex DNAs. Besides, due to their high solubility and electrostatic attraction to phosphate backbone of DNA structure, cationic Pc compounds were employed. The developed biosensor would potentially be used in various fields such as determining DNA in PCR products for the identification of numerous organisms providing *in vivo/in vitro* imaging of double-stranded DNA and G-quadruplex DNA in the future. Thus, imaging of DNA species can give a platform to investigate these species' intracellular functions and interactions, quantifying DNA species *in vivo* conditions and providing DNA imaging in applications such as gel electrophoresis.

With this motivation, phthalocyanine (Pc) integrated mercaptopropionic acid capped quantum dot bio-probe was developed. Its usability was investigated for the quantitative determination of double helix and G-quadruplex DNA in synthetic samples.

2. Materials and methods

All experiments were conducted in pH 7.4 TRIS buffer solution containing 150 mM KCl. Stock oligonucleotide (sequences were given in Table S1) solutions were prepared in buffer solution at the concentration recommended by the manufacturer. The solutions were denatured at 95 °C for 10 min, cooled to room temperature, and stored at +4 °C. The conformation of As1411 was parallel, Tel21 and Tel 45 were hybrid (Fig. S1). **ctDNA** was prepared as 0.001 g/mL and cooled to room temperature after 10 min of denaturation at 95 °C. **ctDNA** concentration was calculated from its absorbance value at 260 nm and the molar absorption coefficient of 6600 $Lmol^{-1}$ cm^{-1}. Stock phthalocyanine (1.5×10^{-4} M) solutions were prepared in buffer solution. The **Pc** solutions were shaken with a circular rotator for at least 24 h for complete dissolution. All solutions were wrapped in aluminium foil to protect them from photocatalytic degradation and stored at room temperature.

2.1. Synthesis of mercaptopropionic acid (mpa@QD) capped quantum dot

Sodium citrate, mercaptopropionic acid, and Te(IV) pH 9 were added to the cadmium chloride solution, respectively. It was heated up to 60 °C. Sodium borohydride was then added to the mixture. It was heated at 90 °C for 30 min with stirring. After cooling, ethanol was added at a ratio of 1:3 and centrifuged for 10 min. The supernatant portions were then discarded, and the formed **mpa@QD** was diluted with distilled water. The stock concentration of **mpa@QD** was 0.4 mM.

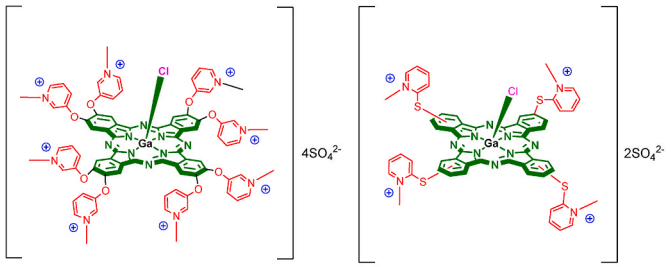

Fig. 1. Chemical structures of the phthalocyanines (a) **Pc1**, (b) **Pc2.**

2.2. Selection of appropriate phthalocyanine compound

To develop the quantum dot-integrated **Pc** biosensor, preliminary experiments were conducted with two phthalocyanine compounds (**Pc1**: 2,3,9,10,16,17,23,24-Octakis-[(N-methyl-3-pyridyloxy)phthalocyaninato] chlorogallium(III) sulphate [25]; **Pc2**: 2(3),9(10),16(17),23(24)-Tetrakis-[(N-methyl-2-mercaptopyridine)phthalocyaninato] chlorogallium(III) sulphate [26]). The molecular structure of the phthalocyanine compounds is given in Fig. 1. The synthesis steps were briefly as follows:

Pc1: A mixture of anhydrous gallium (III) chloride, 4,5-bis(3-pyridyloxy)phthalonitrile and quinoline was stirred at 180 °C for 7 h under nitrogen atmosphere. This compound was precipitated and purified. The product was heated to 120 °C in freshly distilled DMF and excess dimethylsulphate (DMS) was added dropwise. The mixture was stirred at 120 °C for 12 h. The obtained product (**Pc1**) was precipitated and purified [25].

Pc2: A mixture of anhydrous gallium(III) chloride, 4-(2-mercaptopyridine) phthalonitrile, DBU and quinoline was stirred at 180 °C for 7 h under nitrogen atmosphere. This compound was precipitated and purified. The product was heated to 120 °C in freshly distilled DMF and excess DMS was added dropwise. The mixture was stirred at 120 °C for 12 h. The obtained product (**Pc1**) was precipitated and purified [26].

2.3. FT-IR analysis

Pc1, **mpa@QD** and **Pc-mpa@QD** solutions were mixed with high purity KBr. Then, the solution phase was evaporated by heating at 50 °C overnight. The obtained solid was pulverized in agar mortar. Pelletized samples were analyzed by Bruker (Tensor II) FT-IR-spectrophotometer.

2.4. Quenching of the quantum dot

In preliminary experiments, quenching of the quantum dot signal and signal recovery were investigated. The signal recovery studies were conducted with **AS1411**.

2.5. Effect of co-existing substances

The effects of species found in biological materials on the **Pc-mpa@QD** biosensor signal have been investigated. The effect of Zn^{2+}, Mg^{2+}, Ca^{2+}, Na^+ ions, and BSA on the **Pc-mpa@QD** biosensor signal was investigated in the absence of DNA individually.

2.6. Analytical properties of the biosensor

Analytical performance of the developed biosensor for **AS1411**, **Tel21**, **Tel45,** and **ctDNA** detection was investigated. The limit of

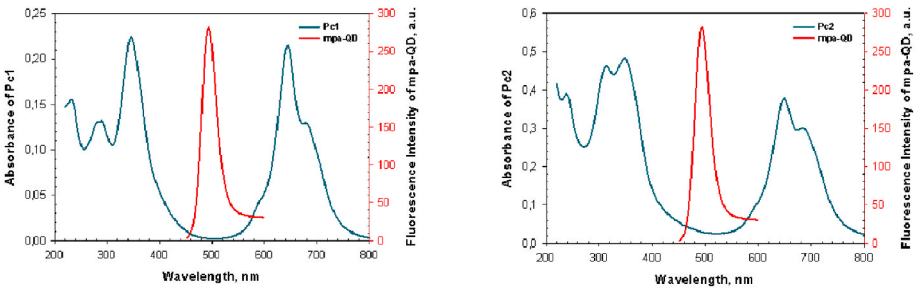

Fig. 2. UV–Vis. spectra of (a)**Pc1**, (b)**Pc2,** and fluorescence spectrum of **mpa@QD** (λ_{ex} = 270 nm, in buffer).

detection and limit of quantification were determined from the formulas $3S_b/m$ and $10S_b/m$, where S_b is the standard deviation of the blank sample, m is the slope of the graph. The linear calibration range was determined, and relative standard deviation % was calculated for different DNA concentrations.

2.7. Application of biosensor in synthetic biological medium

Different synthetic samples were prepared to determine the selectivity and validity of the developed biosensor. Poly(ethylene glycol) 8000 (PEG 8000) simulated the cell environment.

At the presence of a high concentration molecular crowding (HCMC) agent: The biological macromolecules occupy a significant fraction (20–40%) of the cellular volume. Thus, 24% PEG 8000 was prepared and spiked with **AS1411**, **Tel21**, **Tel45,** and **ctDNA**. The recovery values were calculated from the spiked amount.

At the presence of low molecular crowding agent and high concentration of common ions (HCCI): In the second synthetic sample application, synthetic samples that contain a high concentration of Zn^{2+}, Ca^{2+}, Na^{+}, Mg^{2+} (670 μM each), 4% PEG 8000, and BSA were prepared since the conformation of quadruplex DNAs can change in the presence of cations. **AS1411**, **Tel21**, **Tel45,** and **ctDNA** solutions were separately added to the synthetic solution, and the recovery values were calculated from the spiked amount.

The intracellular environment of mammals (IEM): A synthetic sample containing cations at the levels found in mammalian cells was prepared [27]. The synthetic samples containing 24% PEG 8000 as well as 139 mM K^{+}, 12 mM Na^{+}, 4 mM Cl^{-}, 12 mM HCO_3^{-}, 0.8 mM Mg^{2+}, 0.00018 mM Ca^{2+} mimicked the mammalian cell environment. **AS1411**, **Tel21**, **Tel45,** and **ctDNA** (1 μM) were spiked individually, and the recovery values were calculated from the spiked amount. The synthetic sample was added to the sensor medium in which the final concentration of DNA did not exceed the linear range. If necessary, the total youden zero method was used to eliminate the matrix signal when calculating the recovery rates.

3. Results and discussion

3.1. The on-off-on behavior of Pc-mpa@QD

The phthalocyanine integrated mercaptopropionic acid capped quantum dot (**Pc-mpa@QD**) biosensor was developed for the quantitative detection of **AS1411**, **Tel21**, **Tel45**, and **ctDNA** in synthetic biological samples. Herein, **mpa@QD** acts as a fluorophore with a negatively charged functional group and positively charged **Pc** is the DNA recognition probe with its conjugated π electrons (Fig. 1). Integration of these two components with electrostatic attraction causes fluorescence quenching of quantum dots. The process is reversible due to the weak nature of the interaction. The addition of DNA causes strong interactions of DNA with phthalocyanine resulting in a quantum dot being released. The released quantum dot gains the fluorescence property again. DNA and phthalocyanine interaction is stronger than the interaction of **Pc** and **mpa@QD**, mainly due to strong π-π stacking between Pc and DNA. Phthalocyanines are planar aromatic systems, and they can easily interact with the conjugated π biological systems such as double-stranded and G-quadruplex DNA due to their highly conjugated 18- π electron.

3.2. The fluorescence quenching mechanism of mpa@QD with Pc molecules

The fluorescence quenching mechanism of **mpa@QD** with **Pc1 and Pc2** molecules was investigated. No significant spectral overlap was observed between the emission spectrum of mpa@QD and the absorption spectrum of both **Pc1** and **Pc2** molecules (Fig. 2). The quenching of fluorescence intensity of the QDs can be observed due to a variety of molecular interaction, ranging from Förster resonance energy transfer (FRET), excited-state reactions, ground state complex formation, molecular rearrangements and photo-induced electron transfer [12,28]. An efficient overlap between the fluorescence emission spectrum of the donor and absorption spectrum of acceptor should be occurred for FRET. Thus, the energy emission spectrum from the donor fluorophore must overlap with the energy absorption spectrum of the acceptor (quenching agent). Moreover, the efficiency of energy transfer depends upon the extent of overlap between the donor's emission spectrum and the acceptor's spectrum [29]. As shown Fig. 2, there is no efficient overlap between the phthalocyanine compounds and **mpa@QD.** The spectral observations supported that the quenching appears to be through electronic interactions between phthalocyanine compounds and **mpa@QD.** Similar observations were found also in the literature. Barata et al. investigated the interaction of Pc compounds (Pc 64, Pc 62, Pc 63 etc.) with QDs and concluded that to obtain an equivalent quenching of QDs, less molecules of Pc with six charged groups as Pc 64 were needed than for Pc with four charged groups as Pcs 62 or 63 which is an indicator of the electrostatic nature of interactions [30].

3.3. Selection of appropriate phthalocyanine compound

One of the essential points to be considered when developing a phthalocyanine-**mpa@QD** integrated system is the reversibility of the interaction of phthalocyanine and **mpa@QD**. Studies have been carried out with two different phthalocyanines. These two phthalocyanines are effectively quenched on the fluorescence intensity of **mpa@QD**. To obtain detection limits and high analytical sensitivity, it is essential to achieve maximum fluorescence intensity gain by adding the same amount of DNA. In addition, the reproducibility of the results is an important point to consider when optimizing the type and amount of phthalocyanine.

For the quantum dot to integrate with phthalocyanine, the interaction of these two phthalocyanines must decrease the fluorescence intensity of the quantum dots. Considering the analytical performance of the biosensor, the maximum recovery of the fluorescence signal as a

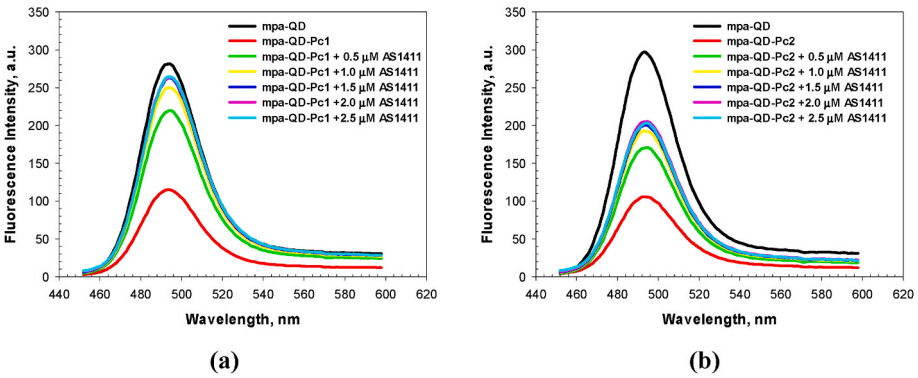

Fig. 3. Fluorescence quenching of **mpa@QD** by adding (a)**Pc1**, (b)**Pc2,** and fluorescence signal gain with AS141.

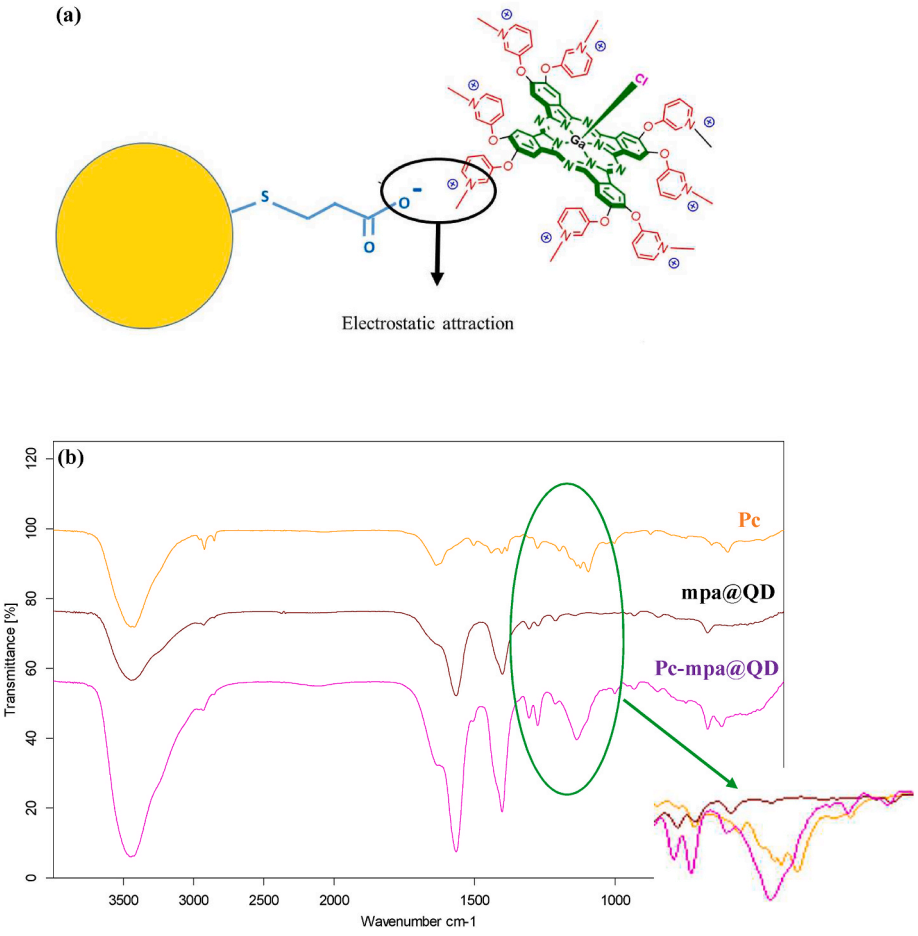

Fig. 4. Interaction mechanism **(a)** and FT-IR spectrums for **Pc1**, **mpa@QD and Pc-mpa@QD (b).**

result of interaction with the biomolecule is essential for the linear range.

Therefore, preliminary studies have been carried out with phthalocyanines that interact with mercaptopropionic acid-coated CdTe. The positive charge of the phthalocyanine interacts with the negatively charged **mpa@QD**. For this reason, cationic phthalocyanines were chosen in this study. It is seen that the **Pc1** compound effectively quenches the fluorescence emission of the quantum dot (Fig. 3). The fluorescence intensity was obtained at around 300 a.u, and it was quenched to around 100 a.u by adding **Pc1**. The addition of 2.5 μM of **AS1411** resulted in fluorescence signal recovery of about 94%. As shown in Fig. 3, the **Pc2** compound also effectively quenched to the fluorescence of the quantum dot. Signal recovery studies show that the recovery was found approximately 64% by adding 2.5 μM of AS1411 to this system. Fluorescence recovery was found higher for **Pc1** by adding the same amount of **AS1411**.

The spectrophotometric titration of **Pc1** with **DNAs** may indicate the end stacking or intercalation of phthalocyanine to G-quadruplex DNA capable of performing as π-π stacking interactions with the G-tetrads due to the large aromatic moiety of phthalocyanine [31]. The redshift in the Soret band of phthalocyanine was observed at around 15 nm, resulting from the intercalation of **Pc1** into G-tetrads [32]. On the other hand, the redshift in the Soret band of **Pc1** was not highly pronounced for **ctDNA,** which might be due to the external binding of **Pc1** to double-stranded

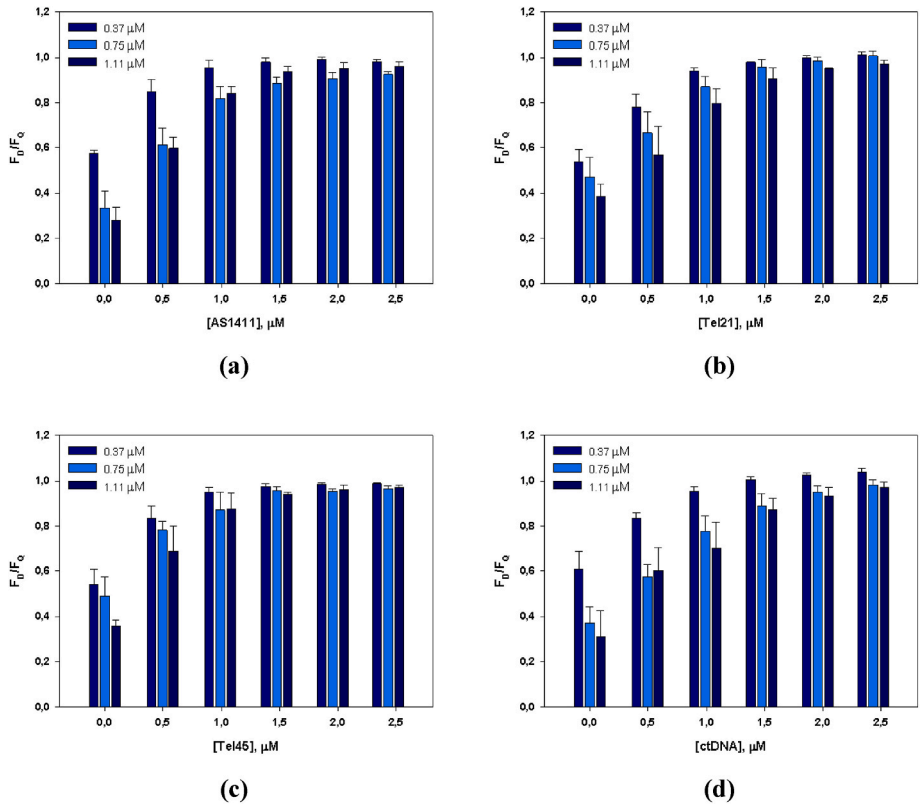

Fig. 5. Effect of **Pc1** concentration on recovery of fluorescence intensity. **Pc1** concentration was arranged between 0.37 and 1.11 μM. All recovery experiments were done for the DNA concentration ranging from 0 to 2.5 μM.

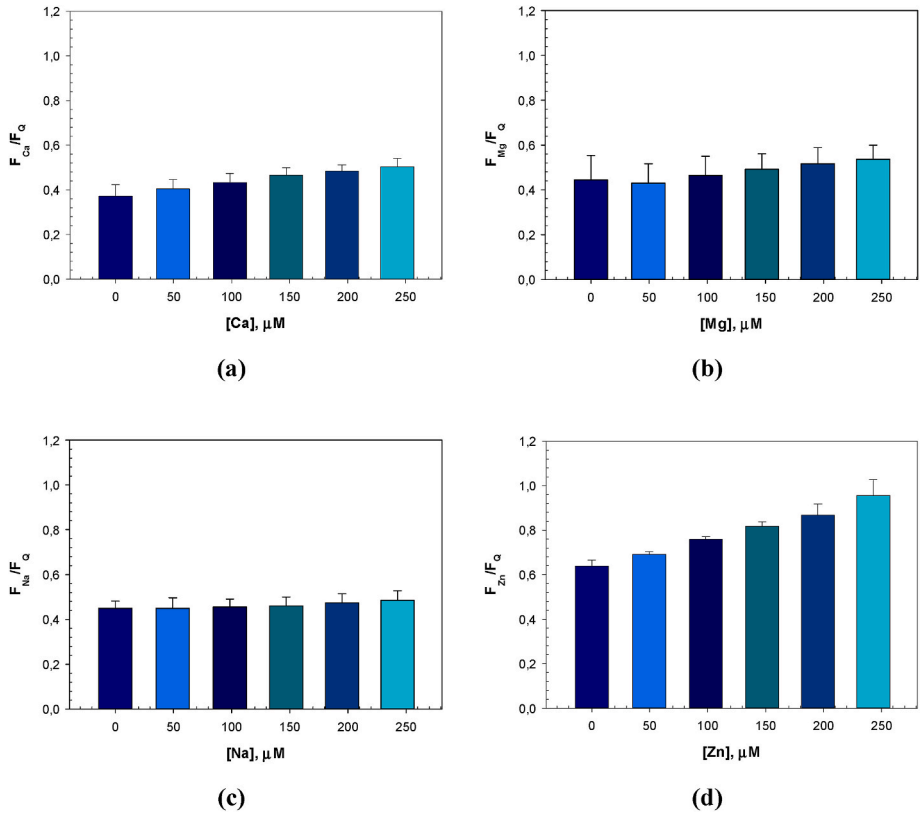

Fig. 6. Effect of different matrix constituents on the fluorescence recovery of **Pc-mpa@QD**. The fluorescence recovery were calculated for the concentration ranging from 0–250 μM of (a) Ca^{2+}, (b) Mg^{2+}, (c)Na^{+} and (d)Zn^{2+} ions.

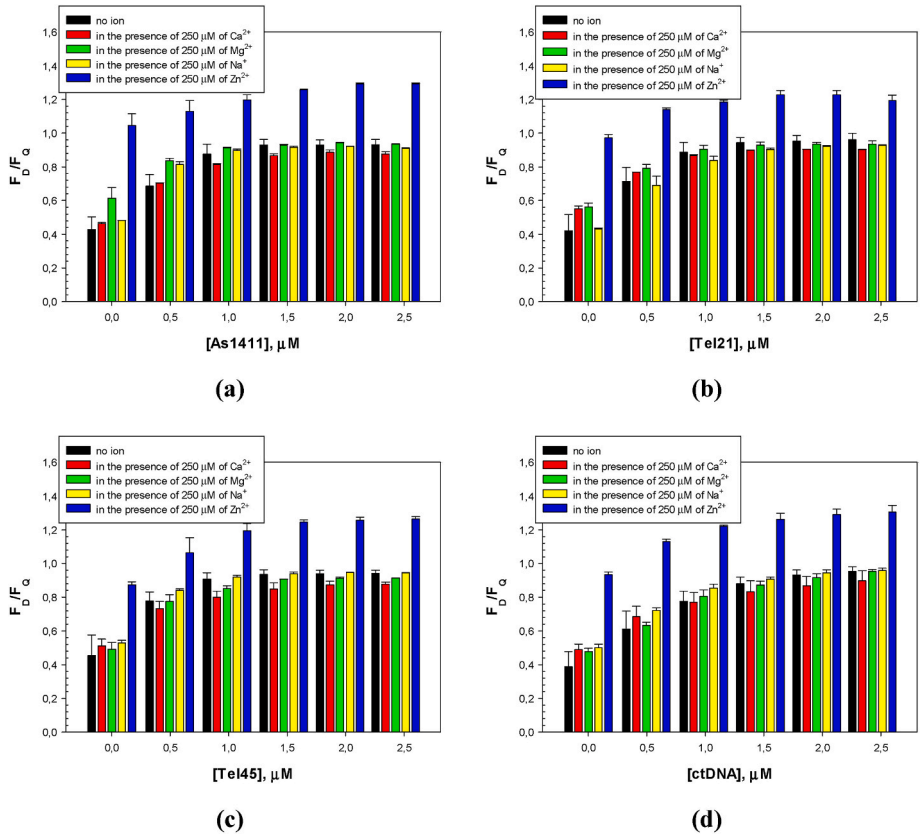

Fig. 7. Fluorescence signal recoveries in the absence and presence of 250 μM of Ca^{2+}, Mg^{2+}, Na^{+} and Zn^{2+} ions, (a) **AS1411**, (b) **Tel21**, (c) **Tel45** and (d) **ctDNA.**

DNA (Fig. S2).

3.4. FT-IR spectra for Pc1, mpa@QD and Pc1-mpa@QD

FT-IR measurements were performed to confirm successful conjugation of **mpa@QD** with **Pc1**. The spectra of the bare **Pc1**, **mpa@QD** and **Pc-mpa@QD** were given in Fig. 4. As for **Pc1**, the vibration bands at around 3422 cm^{-1} were consistent with the N–H, 2923 and 2853 cm^{-1} peaks were corresponding to symmetrical and asymmetrical aliphatic C–H vibrations. The peak at 1636 cm^{-1} was corresponding to the C –C benzene stretching. The weak vibration band at 1285 cm^{-1} was ascribed to C–N bond in plane isoindole ring [33,34]. The vibration band at 1096 cm^{-1} was corresponding to the S═O stretching vibration [35]. The peak is absent in **Pc-mpa@QD** FT-IR speectrum which attributed to the replacement of sulphate with negatively charges **mpa@QD** which indicates the electrostatic attraction.

3.5. The effect of Pc1 concentration

In developing the quantum dot integrated phthalocyanine biosensor, the concentration of phthalocyanine must be optimized to recover the fluorescence signal efficiently. Some important points should be considered when optimizing the concentration of phthalocyanine. First of all, the concentration of phthalocyanine should be high enough to make the linear range wide and, at the same time, low enough to prevent irreversible signal loss. In particular, it may be the case that excessive phthalocyanine compound added to the medium inhibits fluorescent signal recovery. Fig. 5 shows the effect of the concentration of **Pc1** on signal recovery. As shown in this figure, the phthalocyanine concentration did not significantly affect to the fluorescence recovery of the studied range. The recovery values were found high at 0.37 μM of **Pc1**. To decide the optimum concentration, the linear range and the sensitivity data were also taken into consideration, as well as signal repeatability (Fig. S3). Thus, the studies were continued with a **Pc1** concentration of 0.75 μM.

3.6. The effect of co-existing ions on biosensor response

The effect of some common ions on biosensor signals was investigated. The experiments were done in the absence of DNA. The signal recovery values with respect to the increasing amount of ions were given in Fig. 6a–d. F_{Ca}/F_Q, F_{Mg}/F_Q, F_{Na}/F_Q and F_{Zn}/F_Q values increased from 0.37 ± 0.05 to 0.50 ± 0.04 by the addition of 0–250 mM of Ca^{2+}, from 0.44 ± 0.11 to 0.54 ± 0.06 for the same concentration increment of Mg^{2+}, from 0.45 ± 0.13 to 0.49 ± 0.04 for the same concentration increment of Na^{+} and from 0.64 ± 0.03 to 0.96 ± 0.07 for the same concentration increment of Zn^{2+}, respectively. Considering these results, it can be said that the effect of zinc on the biosensor signal is quite high, while the effect of other ions is negligible. Fortunately, zinc concentration is not high in many biomaterials. The enzyme inhibition constants for inhibition of crucial enzymes by zinc may become significant up to 10^{-8} M free Zn^{2+}. Hence, the free cellular Zn^{2+} concentration may be estimated for this order of magnitude [36].

3.7. The effect of Ca^{2+}, Mg^{2+}, Na^{+}, and Zn^{2+} ions on the determination of AS1411, Tel21, Tel 45 and ctDNA

The effect of Ca^{2+}, Mg^{2+}, Na^{+} and Zn^{2+} ions on determination of **AS1411**, **Tel21**, **Tel45** and **ctDNA** was given in Fig. 7a–d. The effect of these ions in all 4 DNA types was found insignificant, except Zn^{2+}. Fortunately, as mentioned above, the concentration of Zn^{2+} is not found high in biological materials.

3.8. The effect of BSA on biosensor response

Bovine Serum Albumin (BSA) is a widely used model protein to

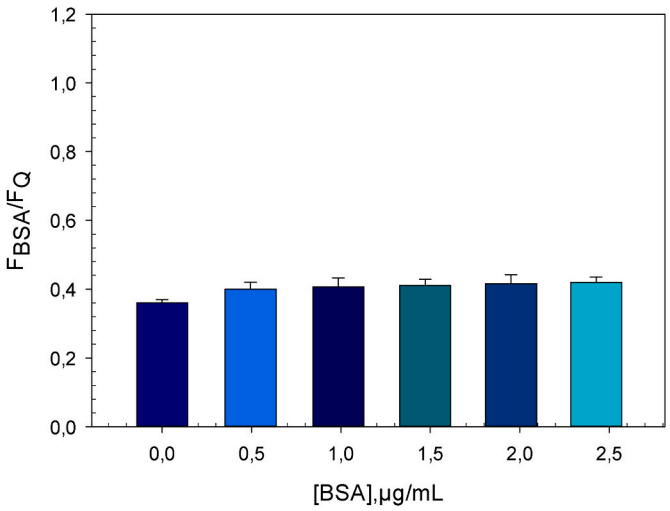

Fig. 8. Effect of BSA on fluorescence recovery of **Pc-mpa@QD**. The fluorescence recovery was calculated for the concentration range of 0–2.5 µg/mL.

evaluate the interactions of different chemical compounds with albumin due to its easy availability, low cost, and structural similarity to Human Serum Albumin (HSA). Albumin is a plasma protein and is found in the blood. Also known as a critical transport protein, it can bind ligands, ions, lipids, drugs, and toxins in acidic and neutral media [37]. The effect of BSA on the signal response of the developed sensor was investigated due to availability of albumin in body fluids.

Fig. 8 shows the effect of BSA concentration on the fluorescence signal. Less than 5% signal increment was obtained, increasing the BSA concentration to 2.5 µg/mL. Thus, it can be said that the effect of BSA is negligible.

3.9. The effect of BSA on the determination of AS1411, Tel21, Tel 45 and ctDNA

The effect of the presence of BSA on the determination of **AS1411**, **Tel21**, **Tel45,** and **ctDNA** is given in Fig. 9a–d. The effect of BSA for all 4 DNA types is found not significant.

3.10. Analytical figures of merit

Analytical properties of the developed biosensor for **AS1411**, **Tel21**, **Tel45,** and **ctDNA** detection were investigated. As seen in Fig. S4, when the **AS1411** concentration increases, the signal gain increases linearly to approximately 0.32 µM. Various analytical properties are calculated for the region where linearity is provided and given in Table 1. As can be seen from this table, the method has a low relative standard deviation (<5%) over a wide range of concentrations. At the same time, the detection and quantification limits were calculated as 0.055 µM and 0.18 µM, respectively for **AS1411**. The signal gain for **Tel21** is linear (r2> 0.96) over the range of 0–0.36 µM **Tel21** concentration. The detection and quantification limits were calculated as 0.061 µM and 0.20 µM, respectively for **Tel21**. The relative standard deviation values for three concentrations in this range were also <5%. The method has lower detection and detection limits for **Tel45** than **AS1411** and **Tel21** analytes. The linear calibration range of the method was found to be 0–0.29 µM under experimental conditions for Tel45. The detection and quantification limits were calculated as 0.038 µM and 0.13 µM, respectively. RSD % values were found to be <5%. Analytical performance characteristics of the developed integrated biosensor for **ctDNA** were also studied. The relative standard deviations of the method for three different concentrations of **ctDNA** were found lower than G-quadruplex DNAs. In addition, the detection and quantification limits are higher than G-quadruplex DNAs (0.091 µM and 0.30 µM, respectively).

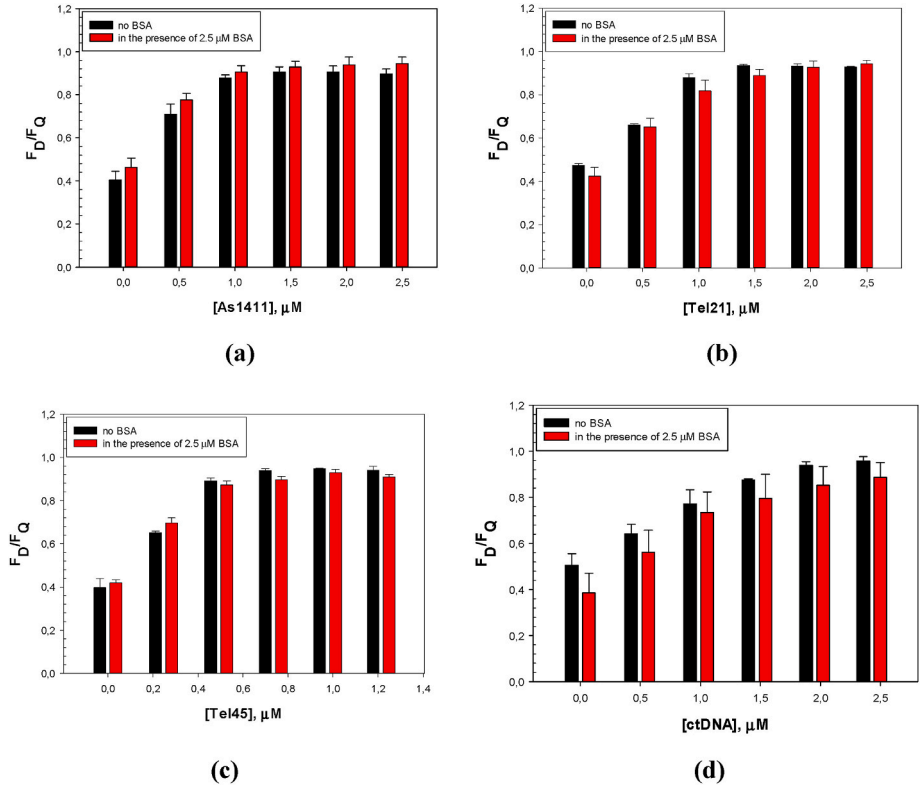

Fig. 9. Fluorescence recovery values in the absence and presence of 2.50 µM of BSA (a) **AS1411**, (b) **Tel21**, (c) **Tel45** and (d) **ctDNA.**

Table 1
The analytical figure of merits.

	AS1411	Tel21	Tel45	ctDNA
Calibration equation	y = 1.37x+ 0.407 (0–0.32 μM)	y = 1.22x +0.429 (0–0.36 μM)	y = 1.95x +0.415 (0–0.29 μM)	y = 0.82x +0.366 (0–0.42 μM)
r^2	0.956	0.969	0.960	0.990
$3S_b/m$	0.055	0.061	0.038	0.091
10 S_b/m	0.18	0.20	0.13	0.30
RSD % (0.02 μM)	1.34	1.99	0.92	9.23
RSD % (0.20 μM)	3.12	0.45	3.01	7.92
RSD % (0.31 μM)	1.61	0.58	2.05	3.89

m: Slope of calibration plot, RSD: Relative standard deviation, Sb: standard deviation of blank (n = 20).

Table 2
Recovery results for DNA in synthetic real samples.

DNA, μM	**HCMC AS1411 Recovery %**	**HCCI Recovery %**	**HCMC Tel21 Recovery %**	**HCCI Recovery %**
0.05	59.41±7.41	−16.60±10.43	86.60±16.99	24.13±34.65
0.10	67.46±5.74	43.32±0.25	90.53±4.34	68.85±11.06
0.15	76.15±9.17	62.02±3.41	115.72±9.37	97.46±12.49
0.19	82.16±9.10	80.61±3.58	119.67±10.00	103.32±12.19
0.24	94.50±6.56	84.29±2.67	111.30±10.64	107.30±8.19
0.29	95.92±8.06	92.57±4.87	111.07±5.61	117.50±6.98
0.33	99.06±5.95	91.45±5.08	106.82±6.51	114.68±3.99
0.38	101.68±1.69	89.82±2.58	103.68±5.70	115.23±1.94
0.43	100.15±2.64	91.32±2.45	109.73±3.83	110.59±2.14
DNA, μM	**HCMC Tel45 Recovery %**	**HCCI Recovery %**	**HCMC ctDNA Recovery %**	**HCCI Recovery %**
0.05	90.47±13.90	72.16±20.83	15.28±17.49	74.28±13.57
0.10	101.62±3.16	118.17±7.16	89.01±22.00	105.89±6.89
0.15	102.94±4.02	108.22±11.68	84.41±12.45	110.07±4.66
0.19	84.09±5.38	100.37±9.11	103.56±13.61	106.68±1.08
0.24	72.46±3.60	101.61±9.13	117.41±17.21	100.52±2.33
0.29	61.47±2.66	89.07±7.67	114.99±13.73	107.03±3.79
0.33	53.64±2.59	77.37±7.41	118.22±12.65	104.57±0.79
0.38	45.64±2.29	68.70±6.59	116.63±8.43	99.51±1.11
0.43	41.32±2.12	60.76±6.07	115.58±10.06	99.22±1.91

Recovery values were low for 0.05 μM concentrations for all four DNA types. However, both recoveries and precision values are acceptable at higher concentrations. The recovery values were found in the range of 90–110%, except for the outside linear range, given in the previous section.

3.11. The application of the developed method on different synthetic samples

The primary motivation of this study is to show the potential usability of the developed phthalocyanine integrated biosensor for the determination of G-quadruplex DNA/double-stranded DNA in complex matrices. Biological sample matrices are generally more complex and crowded than inorganic matrices. Biological samples contain many components such as proteins and minerals. Polyethylene glycol is a preferred compound in the synthetic creation of crowded environments such as cell lysates and interstitial fluids. This compound is used as a "molecular crowding agent" representing biological environments and is thought to represent the complex-crowded-concentrated environment of the biological matrices. In the literature, PEG is used as a molecular crowding agent in G-quadruplex studies. Kan et al. stated that (PEG) induces the formation of a G-quadruplex structure in the guanine-rich strand of telomeric DNA at a K^+ ion concentration that is unable to induce G-quadruplex formation alone [38,39]. In particular, the ability to determine the concentrations of biological analytes such as DNA in different media such as water or buffer is insufficient for many applications because the behavior of many chemicals in a crowded environment is quite different from pure water or buffer environments. Therefore, since such inorganic media will be limited to represent the biological matrix, DNA types were determined in various synthetic samples prepared in the presence of PEG as "molecular crowding agent". A synthetic biological medium was created by adding **AS1411**, **Tel21**, **Tel45** and **ctDNA** to media containing 24% PEG. The concentrations of analytes in these samples were determined by daily prepared calibration graphs. The recoveries were calculated from the known concentrations of the analytes and given in Table 2. The other synthetic samples were prepared to contain a high concentration of ions (Na^+, Mg^{2+}, Ca^{2+}, Zn^{2+}) as well as bovine serum albumin and PEG. The DNA samples were spiked and recovery % was calculated. Calculations were made with the calibration graphics and the effect of the matrix signal was eliminated using the total Youden blank method when calculating the analyte concentrations.

In another application performed in real sample analysis applications, the concentrations of DNA species (1 μM, 2 μM, 3 μM, 4 μM) were determined by preparing different solutions containing **AS1411**, **Tel21**, **Tel45,** and **ctDNA** at different concentrations containing the ions in the intracellular environment at certain concentrations. % recoveries were

Table 3
DNA determination in synthetic intracellular samples (mammalian cell environment) with the developed biosensor.

	Recovery %[a]			
	As1411	Tel21	Tel45	ctDNA
1 μM	79.74 ± 7.71	93.51 ± 4.89	100.38 ± 4.30	60.20 ± 6.94
2 μM	91.52 ± 2.07	92.71 ± 5.10	107.38 ± 0.68	85.24 ± 7.09
3 μM	99.87 ± 1.68	90.27 ± 4.66	114.43 ± 7.41	86.00 ± 7.09
4 μM	89.63 ± 2.19	90.56 ± 7.12	98.67 ± 8.24	80.12 ± 3.62

[a] Concentrations used in calculating the recovery values were calculated with the daily calibration charts prepared with the intracellular solution.

calculated from the DNA concentrations (Table 3). As can be seen from the table, the recovery values are quantitative in the synthetic sample medium representing the cell medium.

4. Conclusion

The results of this investigation show that a quantum dot integrated biosensor has been developed in which the G-quadruplex and double-helix DNA concentration can be determined in various environments. The satisfactory recovery efficiency in synthetic biological samples suggested that the Pc integrated **mpa@QD** biosensor would be a useful sensor in the quantitative determination of DNA samples in the biological matrix. Based on the obtained results, it is thought that the developed biosensor has the potential for the determination of G-quadruplex and double-helix DNA species *in vivo*. The main goal of this work is to develop a new biosensor to detect G-quadruplex and double-stranded DNA. Although the scope of this study includes *in vitro* experiments, preliminary data have been provided for future *in vivo* studies with further studies.

Author contributions

Ayşe Topcu: Performing experimental studies. Esrra Bağda: Design of experiments and interpretation of results, preparation of manuscript. Tülay Oymak: Synthesis of QD and design of experiments and interpretation of results. Mahmut Durmus: Re-synthesis of the compounds.

Acknowledgment

This work was supported by the Scientific Research Project Fund of Sivas Cumhuriyet University (Türkiye) under the project number ECZ-067.

Appendix A. Supplementary data

Supplementary data to this article can be found online at https://doi.org/10.1016/j.ab.2022.114777.

References

[1] A.L. Efros, L.E. Brus, Nanocrystal quantum dots: from discovery to modern development, ACS Nano 15 (4) (2021) 6192–6210.
[2] A.S. Karakoti, R. Shukla, R. Shanker, S. Singh, Surface functionalization of quantum dots for biological applications, Adv. Colloid Interface Sci. 215 (2015) 28–45.
[3] W.Y. William, E. Chang, R. Drezek, V.L. Colvin, Water-soluble quantum dots for biomedical applications, Biochem. Biophys. Res. Commun. 348 (3) (2006) 781–786.
[4] A.F.E. Hezinger, J. Teßmar, A. Göpferich, Polymer coating of quantum dots–a powerful tool toward diagnostics and sensorics, Eur. J. Pharm. Biopharm. 68 (1) (2008) 138–152.
[5] M.A. Farzin, H. Abdoos, A critical review on quantum dots: from synthesis toward applications in electrochemical biosensors for determination of disease-related biomolecules, Talanta (2020), 121828.
[6] F. Ma, M. Liu, C.Y. Zhang, Ligase amplification reaction-catalyzed assembly of a single quantum dot-based nanosensor for sensitive detection of alkaline phosphatase, Chem. Commun. 55 (61) (2019) 8963–8966.
[7] F. Ma, Q. Zhang, C.Y. Zhang, Catalytic self-assembly of quantum-dot-based microRNA nanosensor directed by toehold-mediated strand displacement cascade, Nano Lett. 19 (9) (2019) 6370–6376.
[8] C.C. Li, W.X. Liu, J. Hu, C.Y. Zhang, A single quantum dot-based nanosensor with multilayer of multiple acceptors for ultrasensitive detection of human alkyladenine DNA glycosylase, Chem. Sci. 10 (37) (2019) 8675–8684.
[9] J. Hu, M.H. Liu, C.Y. Zhang, Construction of tetrahedral DNA-quantum dot nanostructure with the integration of multistep forster resonance energy transfer for multiplex enzymes assay, ACS Nano 13 (6) (2019) 7191–7201.
[10] O. Adegoke, T. Nyokong, Unsymmetrically substituted nickel triazatetrabenzcorrole and phthalocynanine complexes: conjugation to quantum dots and applications as fluorescent "Turn ON" Sensors, J. Fluoresc. 24 (2) (2014) 481–491.
[11] O. Adegoke, T. Nyokong, Conjugation of mono-substituted phthalocyanine derivatives to CdSe@ ZnS quantum dots and their applications as fluorescent-based sensors, Synth. Met. 188 (2014) 35–45.
[12] O. Adegoke, T. Nyokong, Effects of analytes on the fluorescence properties of CdTe@ ZnS quantum dots decorated with cobalt tetraamino-phthalocyanine, J. Lumin. 146 (2014) 275–283.
[13] O. Adegoke, T. Nyokong, Fluorescence "turn on" probe for bromide ion using nanoconjugates of glutathione-capped CdTe@ ZnS quantum dots with nickel tetraamino-phthalocyanine: characterization and size-dependent properties, J. Photochem. Photobiol. Chem. 265 (2013) 58–66.
[14] O. Adegoke, T. Nyokong, Probing the sensitive and selective luminescent detection of peroxynitrite using thiol-capped CdTe and CdTe@ ZnS quantum dots, J. Lumin. 134 (2013) 448–455.
[15] O. Adegoke, S. Khene, T. Nyokong, Fluorescence "switch on" of conjugates of CdTe@ ZnS quantum dots with Al, Ni and Zn tetraamino-phthalocyanines by hydrogen peroxide: characterization and applications as luminescent nanosensors, J. Fluoresc. 23 (5) (2013) 963–974.
[16] O. Adegoke, E. Antunes, T. Nyokong, Nanoconjugates of CdTe@ ZnS quantum dots with cobalt tetraamino-phthalocyanine: characterization and implications for the fluorescence recognition of superoxide anion, J. Photochem. Photobiol. Chem. 257 (2013) 11–19.
[17] O. Adegoke, T. Nyokong, A comparative study on the sensitive detection of hydroxyl radical using thiol-capped CdTe and CdTe/ZnS quantum dots, J. Fluoresc. 22 (6) (2012) 1513–1519.
[18] J. Zhou, Y. Yang, C.Y. Zhang, Toward biocompatible semiconductor quantum dots: from biosynthesis and bioconjugation to biomedical application, Chem. Rev. 115 (21) (2015) 11669–11717.
[19] X. Wu, H. Liu, J. Liu, K.N. Haley, J.A. Treadway, J.P. Larson, M.P. Bruchez, Immunofluorescent labeling of cancer marker Her2 and other cellular targets with semiconductor quantum dots, Nat. Biotechnol. 21 (1) (2003) 41–46.
[20] J.K. Jaiswal, H. Mattoussi, J.M. Mauro, S.M. Simon, Long-term multiple color imaging of live cells using quantum dot bioconjugates, Nat. Biotechnol. 21 (1) (2003) 47–51.
[21] X. Gao, Y. Cui, R.M. Levenson, L.W. Chung, S. Nie, In vivo cancer targeting and imaging with semiconductor quantum dots, Nat. Biotechnol. 22 (8) (2004) 969–976.
[22] D. Zhao, Y. Fan, F. Gao, T.M. Yang, Turn-off-on" fluorescent sensor for (N-methyl-4-pyridyl) porphyrin-DNA and G-quadruplex interactions based on ZnCdSe quantum dots, Anal. Chim. Acta 888 (2015) 131–137.
[23] M.Q. Wang, Y. Wu, Z.Y. Wang, Q.Y. Chen, F.Y. Xiao, Y.C. Jiang, A. Sang, G-quadruplex DNA fluorescence sensing by a bis-amine-substituted styrylquinolinium dye, Dyes Pigments 145 (2017) 1–6.
[24] L.N. Zhu, S.J. Zhao, B. Wu, X.Z. Li, D.M. Kong, A new cationic porphyrin derivative (TMPipEOPP) with large side arm substituents: a highly selective G-quadruplex optical probe, PLoS One 7 (5) (2012), e35586.
[25] M. Camur, V. Ahsen, M. Durmuş, The first comparison of photophysical and photochemical properties of non-ionic, ionic and zwitterionic gallium (III) and indium (III) phthalocyanines, J. Photochem. Photobiol. Chem. 219 (2–3) (2011) 217–227.
[26] M. Durmuş, V. Ahsen, Water-soluble cationic gallium (III) and indium (III) phthalocyanines for photodynamic therapy, J. Inorg. Biochem. 104 (3) (2010) 297–309.
[27] H. Lodish, A. Berk, S.L. Zipursky, et al., Molecular Cell Biology, fourth ed., W. H. Freeman, New York, 2000.
[28] J.F. Callan, R.C. Mulrooney, S. Kamila, B. McCaughan, Anion sensing with luminescent quantum dots–a modular approach based on the photoinduced electron transfer (PET) mechanism, J. Fluoresc. 18 (2) (2008) 527–532.
[29] Z. Liang, M. Kang, G.F. Payne, X. Wang, R. Sun, Probing energy and electron transfer mechanisms in fluorescence quenching of biomass carbon quantum dots, ACS Appl. Mater. Interfaces 8 (27) (2016) 17478–17488.
[30] J.F. Barata, M.G.P. Neves, P.S. Lacerda, P. Conceição, T. Trindade, Quantum dot phthalocyanine non-covalent assemblies–A review, Dyes Pigments 198 (2022), 109931.
[31] J. Lopes-Nunes, J. Carvalho, J. Figueiredo, C.I. Ramos, L.M. Lourenço, J.P. Tomé, C. Cruz, Phthalocyanines for G-quadruplex aptamers binding, Bioorg. Chem. 100 (2020), 103920.
[32] T. Qin, K. Liu, D. Song, C. Yang, H. Su, Porphyrin bound to i-motifs: intercalation versus external groove binding, Chem.–Asian J. 12 (13) (2017) 1578–1586.
[33] E. Elesh, Z. Mohammed, Morphological, linear and nonlinear properties of gallium phthalocyanine chloride annealed thin films, Optik 219 (2020), 165176.
[34] E. Elesh, Z. Mohamed, M.S. Dawood, Temperature dependence of structure, morphology and dielectric characterization of gallium phthalocyanine chloride discs, J. Electron. Mater. 49 (4) (2020) 2633–2641.
[35] C.Y. Boyar, M. Çamur, Novel water soluble 7-oxy-4-(pyridine-3-yl) coumarin substituted phthalocyanines as potential photosensitizers for photodynamic therapy, Inorg. Chim. Acta. 494 (2019) 30–41.
[36] D. Beyersmann, H. Haase, Functions of zinc in signaling. proliferation and differentiation of mammalian cells, Biometals 14 (3) (2001) 331–341.
[37] P. Szymaszek, P. Fiedor, A. Chachaj-Brekiesz, M. Tyszka-Czochara, T. Świergosz, J. Ortyl, Molecular interactions of bovine serum albumin (BSA) with pyridine derivatives as candidates for non-covalent protein probes: a spectroscopic investigation, J. Mol. Liq. 347 (2022), 118262.
[38] Y. Xue, Z.Y. Kan, Q. Wang, Y. Yao, J. Liu, Y.H. Hao, Z. Tan, Human telomeric DNA forms parallel-stranded intramolecular G-quadruplex in K+ solution under molecular crowding condition, J. Am. Chem. Soc. 129 (36) (2007) 11185–11191.
[39] Z.Y. Kan, Y. Yao, P. Wang, X.H. Li, Y.H. Hao, Z. Tan, Molecular crowding induces telomere G-quadruplex formation under salt-deficient conditions and enhances its competition with duplex formation, Angew. Chem. Int. Ed. 45 (10) (2006) 1629–1632.